Published in Journal of Molecular Liquids 425 (2025) 127273
https://doi.org/10.1016/j.molliq.2025.127273

Interfacial Dilational Rheology of Chitosan-Silica Nanocomposite Films at the Aqueous Dispersion/Air Interface

*Carlo Carbone, Iván Navarro-Arrebola, Francisco Ortega, Libero Liggieri, Ramón G. Rubio, Eduardo Guzmán**

Carlo Carbone
Departamento de Química Física, Facultad de Ciencias Químicas, Universidad Complutense de Madrid. Plaza de la Ciencias 2, 28040-Madrid (Spain)
Current Address: Istituto di Chimica della Materia Condensata e di Tecnologie per l'Energia-UOS Genova, Consiglio Nazionale delle Ricerche. Via De Marini 6, 16149-Genova (Italy)

Iván Navarro-Arrebola
Istituto di Chimica della Materia Condensata e di Tecnologie per l'Energia-UOS Genova, Consiglio Nazionale delle Ricerche. Via De Marini 6, 16149-Genova (Italy)
Dipartamento di Chimica e Chimica Industriale. Università degli Studi di Genova. Via Dodecaneso 31, 16146-Genova (Italy)

Libero Liggieri
Istituto di Chimica della Materia Condensata e di Tecnologie per l'Energia-UOS Genova, Consiglio Nazionale delle Ricerche. Via De Marini 6, 16149-Genova (Italy)

Francisco Ortega, Ramón G. Rubio, Eduardo Guzmán
Departamento de Química Física, Facultad de Ciencias Químicas, Universidad Complutense de Madrid. Plaza de la Ciencias 2, 28040-Madrid (Spain)
Instituto Pluridisciplinar, Universidad Complutense de Madrid. Paseo Juan XXIII 1, 28040-Madrid
E-mail: eduardogs@quim.ucm.es

Abstract.

This study investigates the interaction between positively charged chitosan and anionic hydrophilic silica nanoparticles in aqueous media, resulting in the electrostatic formation of chitosan-capped silica nanoparticles. Optimal conditions for the formation of stable dispersions were determined, highlighting that the adsorption of chitosan on silica nanoparticles, as well as its solubility, is enhanced in acidic medium (pH=4.5). Electrophoretic mobility measurements confirmed the positive zeta potential of chitosan-capped particles, indicating charge inversion due to chitosan adsorption on negatively charged silica surfaces. Adsorption at the dispersion/air interface significantly reduces the interfacial tension, with a synergistic effect observed between chitosan and silica. Capillary wave experiments demonstrated the formation of viscoelastic layers with the dilatational elastic modulus of the nanocomposite layers exceeding their viscous modulus. The frequency dependence of the interfacial dilational moduli showed that increasing particle concentration enhanced the viscoelastic properties of the interface. This study provides novel insights into the dilational rheological response of chitosan-capped silica nanoparticle layers, revealing the interplay between surface charge neutralization, adsorption dynamics, and the viscoelastic properties of the interface. The results suggest potential applications in the stabilization of liquid and solid foams and highlight the importance of chitosan-capped particles in modifying water/air interface properties and improving the rheological behavior of particle-laden interfaces.

Keywords: chitosan; electrocapillary waves; interfacial rheology; interfacial tension; silica nanoparticles

1. Introduction

Particle-laden liquid/fluid interfaces are widely studied systems in academia and industry. This is partly due to their key role in the stabilization of dispersed systems such as foams, Pickering emulsions and thin films [1–4]. However, even though particle trapping at the liquid/fluid interface can be considered nearly irreversible in most cases with a trapping energy exceeding the thermal energy,[5,6] the formation of particle-laden films is not always trivial because the transport and trapping of particles at the interface depends on several variables, including the particle density, which can force particle sedimentation. This hydrophilic/hydrophobic balance is defined by their wettability, which determines their penetration at the interface.[6–8] The latter is accounted for by the particle contact angle at the fluid interface, which strongly influences the equilibrium situation of the particle-laden interface.[8–10] Unfortunately, many particles exhibit extreme wettability, such as silica nanoparticles, and commonly remain dispersed in one of the continuous phases rather than adsorbing at the fluid/fluid interface,[7,11–14] requiring their surface modification to provide optimal wettability for adsorption at the fluid/fluid interface.[9,14]

Surface modification of colloidal particles is often based on the binding of ligands to the particles to impart a new functionality.[14,15] There is a wide range of ligands that have been used to modify the surface properties of colloidal particles. These can be attached to the particle surface by a true chemical bond, i.e., covalently, as in the case of silanization of silica surfaces or thiolation of noble metals,[16,17] or they can be bound by weaker molecule-particle interactions, such as electrostatic interactions, hydrogen bonding, or van der Waals forces.[18–20] In the particular case of silica nanoparticles, the electrostatic interaction of dissociated silanol groups with cationic surfactants or polymers, or the interaction by hydrogen bonding between the non-dissociated silanol group on the silica surface and the agent used to modify the silica surface can help to modify the wettability of silica surfaces.[20–27] In the last two decades, health and environmental issues have become increasingly important, so companies are looking to use particles and polymers of natural origin.[28–30]

Chitosan, a natural polysaccharide derived from chitin (the second most abundant polymer on Earth), has been shown to be an effective modifier of the surface properties of materials due to its biocompatibility, biodegradability, and functional versatility.[31,32] When applied to silica surfaces, chitosan can introduce amino and hydroxyl groups, thereby modifying the particle wettability, adsorption capacity, and interaction with biological molecules. Therefore, the use

of chitosan as a capping agent not only improves nanoparticle dispersibility and stability but also enables surface modification, which is critical for applications. The result of the surface functionalization tailored by selecting the fraction and distribution of monomers containing amino and acetamide groups, as well as the pH of the medium, which is very suitable to obtain particles with characteristic selected at will for applications in drug delivery, catalysis, and environmental remediation.[33] Furthermore, the ease of chitosan's chemical modifications allows for tunable surface characteristics, making it an attractive option for improving the performance and functionality of silica-based materials in diverse fields.[34] For instance, Allison et al.[27] proposed the use of chitosan to modify the wettability of silica nanoparticles as a tool for stabilization of edible Pickering emulsions. They found that the electrostatic interaction between cationic chitosan and silica nanoparticles contributes to increase the hydrophobicity of silica nanoparticles and their adsorption to oil/water interfaces. This finding agrees with the modification of the zeta potential (ζ potential) reported by Heidari et al.[35] Furthermore, chitosan-capped silica nanoparticles can organize with different structures at the oil/water interface, resulting in viscoelastic films or agglomerated particle networks depending on the chitosan concentration. This has a significant effect on the rheological properties of the particle-laden fluid/fluid interface. In a more recent work, Allison et al.[26] demonstrated that the stabilization of Pickering emulsions stabilized by chitosan-capped particles can be tuned by pH changes, allowing for the modulation of the chitosan-silica interaction, and consequently the adsorption of the modified particles at the water/oil interface. It is important to note that while the capacity of chitosan-capped particles to adsorb at fluid/fluid interfaces is well documented, particularly in the context of Pickering emulsion stabilization,[26,27,35–38] there is a lack of knowledge regarding the interaction of this type of colloidal system with water/air interfaces. In addition to their utility in the stabilization of interface-dominated systems, chitosan-capped silica nanoparticles may also be employed as drug carriers, taking advantage of their pH-responsive nature.[39]

Based on the above discussion, the adsorption of chitosan onto silica nanoparticles may be used to modulate the hydrophobicity and surface charge of the resulting chitosan-capped nanoparticles. This modification may enhance nanoparticle dispersion stability, thereby allowing the creation of stable, nanoparticle dispersions. Moreover, these stable chitosan-capped silica nanoparticles may present enhanced adsorption at the air/water interface due to increased surface activity compared to either component alone. In this context, the objective of this study is to investigate the adsorption of chitosan-modified hydrophilic silica nanoparticles at the aqueous dispersion/air interface. It is expected that the adsorption of chitosan-capped

silica nanoparticles at the aqueous dispersion/air interface may result in a significant decrease in the interfacial tension and the formation of viscoelastic layers, which make this system a promising candidate for stabilizing foams. By forming robust viscoelastic layers, these nanoparticles can prevent film rupture, retard drainage, and inhibit coalescence, which are essential mechanisms for stabilization. Therefore, understanding the interplay between adsorption and the interfacial rheology of these systems is key to optimizing the performance of particle-laden interfaces. To this aim, silica nanoparticles are modified via direct electrostatic interactions with chitosan chains. This requires the evaluation of the optimal conditions under which chitosan and silica can interact to form stable dispersions, which can be influenced by the strong pH-responsiveness of chitosan. Indeed, the solubility of chitosan in water is very limited, necessitating acidic conditions for its solubilization. Furthermore, increasing the pH to values close to neutrality results in a reduction of the quality of water as a solvent for chitosan.[40] Conversely, silica nanoparticles maintain a negative charge over a pH range of 4 to 9 due to deprotonation of their surface silanol groups. Based on the above discussion, we first evaluate the interaction between chitosan and silica nanoparticles, and the stability of the resulting dispersions at different pH conditions, and then, once the optimal conditions are selected, we study the adsorption of the chitosan-capped particles at the aqueous dispersion/air interface and the high-frequency dilatational rheological response of the formed layers by using electrocapillary wave damping measurements. This systematic study can pave the way for the use of chitosan-capped particles to modify the properties of water/air interfaces, which could have significant on the stabilization of liquid and solid foams.

2. Materials and Methods

2.1. Chemicals

Commercial chitosan (reference 448869) with a molecular weight around (83±14) kDa determined from viscosity measurements, and a deacetylation degree in the range 75-85% was purchased from Merck (Darmstadt, Germany). Silicon dioxide nanoparticles (Levasil® CS30-316P) was supplied by Nouryon (Amsterdam, The Netherlands). It consists of a stable, aqueous dispersion (pH=8-9) of negatively charged amorphous silicon dioxide colloidal nanoparticles (concentration 30%w/w) with an average diameter in the range 10-15 nm. Acetic glacial acid and sodium hydroxide (purity >99.9%) for adjusting pH were purchased from Fisher Scientific (Hampton, NH, USA).

Ultrapure deionized water of Milli-Q quality, with resistivity >18 MΩ·cm, and a total organic content of <6 ppm, obtained using a AquaMAX™-Ultra 370 Series multi-cartridge purification

system (Young Lin Instrument Co., Ltd., Gyeonggi-do, South Korea) was used for cleaning and solution preparation.

2.2. Chitosan solution preparation

A stock solution of chitosan with a concentration of 20 mM was prepared. The required amount of chitosan was weighed and poured into a flask, which was then partially filled with water. Then, 100 μL of glacial acetic acid was added to the flask to lower the pH and ensure complete dissolution of the chitosan. The pH of the resulting aqueous chitosan solution was then adjusted to 4.5 by dropwise addition of 10^{-2} mM sodium hydroxide solution. Finally, the volume of the solution was brought to the desired final value by adding the required amount of dilute aqueous acetic acid solution at pH=4.5.

2.3. Chitosan-silica nanoparticles dispersion preparation

The mixed chitosan-silica dispersion was prepared by a 1:1 dilution according to the procedure described by Ravera et al.[41] Briefly, a chitosan solution (pH=4.5) at twice the concentration of the final mixed dispersion was added dropwise to a stirred suspension of silica nanoparticles at twice the concentration of the final mixed dispersion. This method minimizes potential concentration gradients that could drive the system out of equilibrium.[42,43] Once the mixed dispersion is prepared, the pH is adjusted to 4.5 by adding acetic acid or sodium hydroxide. The dispersion obtained is stirred at 1000 rpm for 30 minutes to ensure thorough homogenization and then allowed to stand overnight. The single-phase or phase-separated character of the dispersions was then assessed by the absence or presence of a sedimented solid phase at the bottom of the container together with a diluted aqueous phase. For the purpose of the present study, only single-phase dispersions were considered.

2.4. Techniques

The effective charge density of the chitosan-capped silica particles was determined from electrophoretic mobility (u_e) measurements using laser Doppler velocimetry. These measurements were performed using a Nanosizer ZS (Malvern Instruments, Malvern, UK). According to Henry's equation, electrophoretic mobility is directly related to the zeta potential (ζ).[44]

The bulk viscosity of the samples was measured using an Ubbelohde viscometer. The liquid samples were placed in a glass viscometer maintained at 23°C. The liquid was then drawn up through a capillary and a measuring bulb, and the time taken for the liquid to fall through the bulb was recorded. The viscometer was calibrated using filtered Milli-Q water, and each sample was filtered prior to testing. The determination of viscosity is based on the principle that the

flow time is directly proportional to the viscosity and inversely proportional to the density of the solution.

The interfacial tension at the air/dispersion interface was determined using a K10T Digital Tensiometer (KRÜSS GmbH, Hamburg, Germany) equipped with a platinum Wilhelmy plate contact probe (contact area of 40.5 mm). Prior to each measurement, the platinum plate was cleaned with ethanol and Milli-Q water, followed by burning with an ethanol torch to remove any residual organic matter. Samples were placed in a glass cuvette that was cleaned with ethanol and Milli-Q water prior to use. The temperature was maintained at 23°C using a thermostatic bath for all measurements. Each data point reported represents the average of at least three independent measurements. Experiments were run long enough to ensure that a steady state interfacial tension was reached.

A home-built electrocapillary wave device was used to determine the dilational rheological properties of the particle-laden fluid/fluid interface at high frequencies (in the range of 10-10^3 Hz). Further details on this technique can be found in previous works.[45,46], and a detailed description of the instrument is reported in reference [47].

3. Results and Discussion

3.1. Chitosan Adsorption on Silica Nanoparticles

The adsorption of chitosan on silica nanoparticles results in a modification of the hydrophobicity of the nanoparticles. This phenomenon is dependent on the pH value which modulates the charge of the chitosan capping layer. Indeed, a decrease in the pH from values close to 9 down to 4 results in an increase in the cationicity of the chitosan, i.e., the degree of positive charge. This is due to the protonation of the amine groups. Accordingly, an effective approach to investigating the binding of chitosan to silica nanoparticles is to work at a pH below the pK_a of chitosan (5.5), where chitosan is highly charged and soluble in water, given that silica nanoparticles are negatively charged within the pH range of 4-9.[26] Based on the above discussion, a pH=4.5 was selected for evaluation the adsorption of chitosan on silica nanoparticles, and the stability of the resulting dispersions. It is therefore possible to select the optimal compositions that result in stable dispersions of particles that can adsorb at the fluid/fluid interface. It is important to note that the maximum adsorption of chitosan on silica surfaces is expected to occur within the pH range 4-pK_a.[26] **Figure 1a** shows the compositional map as a function of chitosan concentration (c_{CHI}) and silica nanoparticle concentration (c_{NPs}) diagram for dispersions of chitosan-capped silica nanoparticles at pH=4.5. The stability of the samples is indicated in terms of the stability time ($t_{stability}$). Thus, the smaller the value of $t_{stability}$

the lower the stability of the dispersions. In the case of the most stable dispersions, they do not show any evidence of phase separation/sedimentation even after 7 weeks of aging. It must be stressed that there are available a series of tools, including measurements of the turbidity or optical density of the samples, that may allow a semiquantitative determination of the phase boundaries in the here studied mixture. However, we consider that for the context of the work, it is enough to identify the compositional regions where the mixtures exhibit instability as instable systems are not suitable for the stabilization of the interface. Therefore, including a more detailed quantification of turbidity or compositional mapping would not significantly advance our understanding of interfacial behavior, which remains the central focus of the work. The compositional map shows that the interaction between chitosan and silica nanoparticles results in the formation of two regions of stability, which are characterized by the single-phase character of the dispersions obtained for the corresponding compositions. The composition of the first region is characterised by a relatively low concentration of chitosan, which results in an incomplete neutralisation of the charges corresponding to the nanoparticles. Therefore, it is expected that the properties of particles obtained in this region can be reminiscent from that of bare silica. Thus, considering their relative highly hydrophilicity, particle belonging to this region will not be considered in this work due to their limited potential to adsorb at the air/dispersion interface. In contrast, within the second region, there is a high concentration of chitosan, which results in the formation of complexes with their charges determined by the excess of chitosan adsorbed on the surface of the silica nanoparticles (see **Figure 1b**). The two regions, which result in the formation of stable dispersions, are separated by a region where the dispersions obtained are not stable and undergo a rapid phase separation within 2 minutes after preparation. This aging process is particularly important in dispersions with compositions situated at the boundary between single-phase regions and phase separation region (represented by triangles and squares in Figure 1a). These dispersions may initially appear to be single-phase mixtures, but they undergo phase separation within a time-scale that range from a few hours after their preparation to several weeks. In Figure 1a, the worsening of the stability as the composition is close to the region where samples undergo a rapid phase-separation is indicated by symbols with darker green or blue tones for the compositional region where chitosan and silica nanoparticles dominate the properties of the dispersions, respectively. The most stable dispersions, represented in Figure 1a by circles with brigth green or blue tones, remain stable for more than 7 weeks after their preparation. It is worth noting that both chitosan solutions and silica dispersions at pH=4.5 remain stable across the entire compositional range studied.

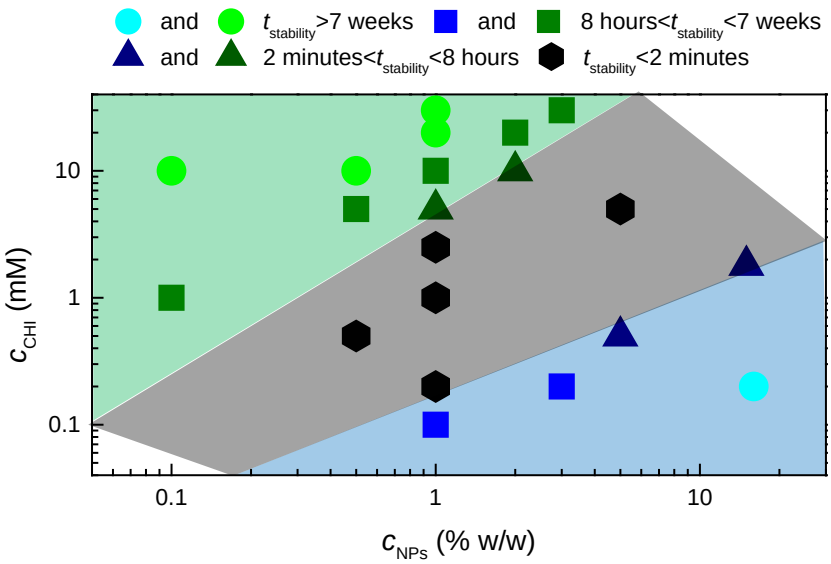

(a)

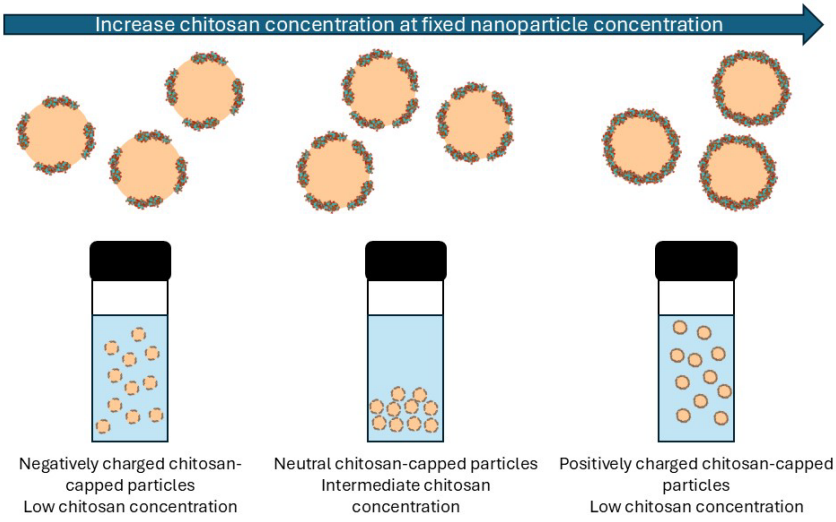

(b)

Figure 1. (a) c_{CHI}-c_{NPs} compositional maps where the stable or instable characters of mixed dispersions including chitosan and silica nanoparticles at pH=4.5 are shown as function of the stability time ($t_{stability}$). Different symbols and colour tone are used for represent dispersions with different $t_{stability}$. Green and blue symbols correspond to dispersions that mantain if single-phase mixtures for more than 2 minutes and grey symbols correspond to phase-separated mixtures that undergo phase-separation in a time smaller than 2 minutes. The shadowed regions indicate the different stability/instability regions in the compositional map, the colour code is the same that for the symbols. Note that the defined timescale represents the maximum stability observed for the samples when considering unstable dispersions. For stable samples, it indicates the longest experimental observation period, after which the samples remain stable. (b) Sketch of the different association and stability of chitosan-capped silica nanoparticles with the increase in the chitosan concentration at a fixed particle concentration.

A better understanding of the characteristics of the chitosan-capped nanoparticles can be obtained by studying their surface charge. This is possible through measurements of electrophoretic mobility that give information on the ζ potential of the particles. **Figure 2** shows the dependence of the ζ potential on the silica nanoparticles concentration for dispersions with different chitosan concentrations. It is crucial to highlight that the determination of the ζ potential is only feasible for dispersions that are stable. This can be rationalized by considering that samples with a composition corresponding to the phase separation region undergo a sedimentation process that competes with their electrophoretic motion, which in turn leads to the occurrence of physically unsound ζ potential values. This substantially reduces the number of measured data in relation to the extension of the compositional map.

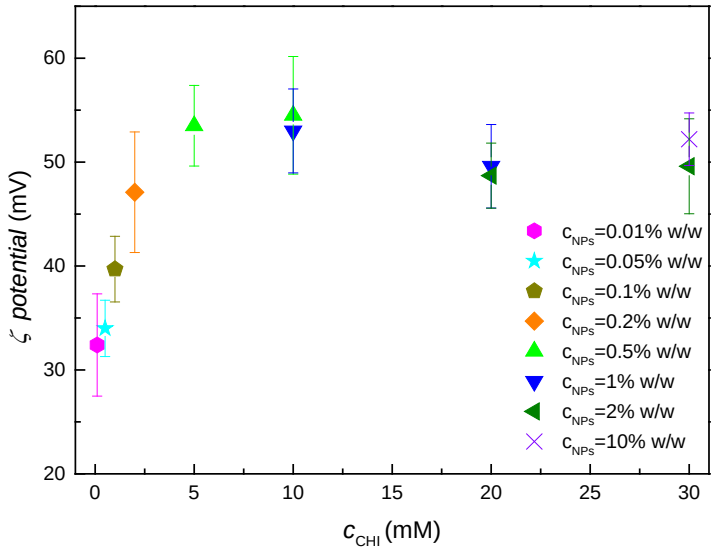

Figure 2. Dependence of the ζ potential on the chitosan concentration for dispersions with different silica nanoparticles concentrations at pH=4.5. The data reported correspond to the average of five independent measurements.

A more detailed examination of the compositional map in terms of the ζ potential indicates that the binding of chitosan to silica nanoparticles is mediated by a process of charge neutralization. Indeed, given that pristine silica nanoparticles posses a negative charge, as evidenced by the value of the ζ potential around (-42±5) mV, and the positive values of the ζ potential for the dispersions of the mixed systems, it is evident that chitosan is adsorbed on the surface of the negatively charged silica nanoparticles. Therefore, for a fixed particle concentration, as the chitosan concentration increases, the adsorption of chitosan on the silica surface results in the neutralization of the negative charge of the nanoparticle surface up to the state of zero net charge, i.e., the isoelectric point. At this point, the nanoparticles lack colloidal stability and therefore

the chitosan-capped particles sediment as a solid phase, leaving a dilute liquid phase, which mainly contains chitosan as supernatant (see **Figure 1b**).[26] Further increases in the chitosan concentration beyond the isoelectric point result in a charge inversion process leading to the production of overcharged chitosan-capped particles, which are characterized by their positive charge. This scenario, sketched in **Figure 1b**, explains the phase behavior of aqueous dispersions of chitosan-capped silica nanoparticles at pH=4.5 at a fixed nanoparticles concentration. The increase in nanoparticle concentration shifts the phase transitions between the different regions of the compositional map to higher values of the chitosan concentration. This may be understood by considering that the increase in the concentration of nanoparticles results in a number of negative charge to neutralize by chitosan addition. This makes it neccessary that the number of chitosan charged monomers also increases. It is noteworthy that analogous behavior has been observed in a multitude of colloidal systems assembled through electrostatic interactions, including polyelectrolyte multilayers, oppositely charged polyelectrolyte-surfactant mixtures and interpolyelectrolyte complexes, among others.[42,48–50]

3.2. Adsorption on chitosan-capped silica nanoparticles at the dispersion/air interface

The characterization of the adsorption of chitosan-capped silica nanoparticles at the aqueous dispersion/air interface was conducted through the measurement of the equilibrium interfacial tension of the aqueous dispersion/air interface and the evaluation of the dilational properties of the particle-laden interface, which was obtained by evaluating the interfacial damping of electrocapillary waves. It should be noted that the bulk characterization was performed over a broader range of particle and chitosan concentrations compared to the interfacial studies. This reduction in the experimental window for interfacial studies results from the experimental challenges associated with interfacial measurements at high concentrations, particularly due to the increased viscosity of the samples and the potential for phase separation. Such aspects can affect the accuracy and reliability of interfacial measurements. Therefore, the concentration ranges explored by each technique have been to ensure meaningful and precise results for each technique. **Figure 3a** shows the dependence of the interfacial tension of the aqueous dispersion/air interface on the silica nanoparticles concentration in dispersions with varying chitosan concentrations. It is noteworthy that bare silica nanoparticles are extremely hydrophilic, and their surface activity is almost negligible. On the other hand, it should be noted that the present study was limited to the investigation of the adsorption of stable dispersions. This can be understood by considering that samples undergoing phase separation present an interfacial tension that depends on their age. In particular, when a complete sedimentation occurs, the

interfacial tension will be close to that corresponding to a diluted chitosan solution from which particles are completely depleted. Therefore, for the purposes of our work on particle-laden interfaces, these measurements do not provide any additional insight into the understanding of the behavior of capped particles at the dispersion/air interface.

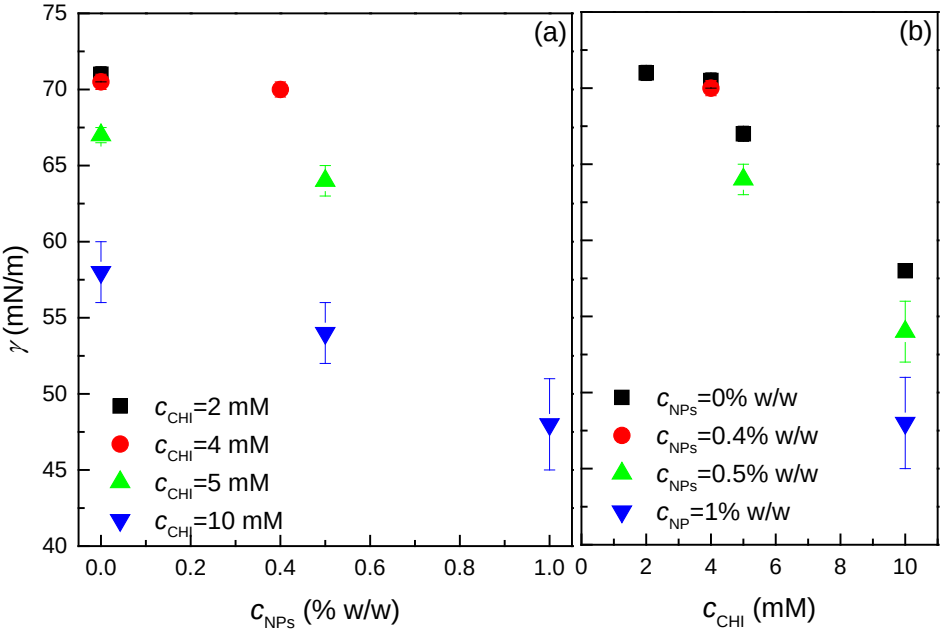

Figure 3. (a) Dependence of the interfacial tension of the aqueous dispersion/air interface on the silica nanoparticles concentration for dispersions at pH=4.5 with different chitosan concentrations. (b) Dependence of the interfacial tension of the aqueous dispersion/air interface on the chitosan concentration for dispersions at pH=4.5 with different silica nanoparticles concentrations. The data reported correspond to the average of three independent measurements.

In contrast to the aforementioned phenomenon for silica nanoparticle adsorption, chitosan exhibits a concentration-dependent surface activity (see **Figure 3b**). The adsorption of chitosan at the aqueous solution/air interface results in a decrease in the interfacial tension, which varies from values close to those corresponding to a pure water/vapor interface (~72 mN/m) for the lowest chitosan concentrations to values below 60 mN/m for the highest concentration studied (10 mM). This can be understood by considering that chitosan presents a certain degree of amphiphilicity as a result of the two types of monomers existing within the chains. The chitosan utilized in this study is a random copolymer comprising, in a molar ratio of 80:20, hydrophilic 2-amino-2-deoxy-β-D-glucose monomers, which are positively charged at the pH of this study, and a series of more hydrophobic N-acetyl-2-amino-2-deoxy-β-D-glucose monomers, which do not present a charge. The latter plays a pivotal role in regulating the adsorption of chitosan at the aqueous solution/air interface.[51] The findings concerning to the adsorption of chitosan

at the water/vapor interface are in agreement with those previously reported by Babak et al.[52] Their results indicated minimal adsorption at highly dilute concentrations and a notable increase in adsorption as the concentration exceeded 10^{-2} mM.

The results demonstrate that the adsorption of chitosan-capped particles at the aqueous dispersion/air interface is enhanced when both the particle and chitosan concentrations are increased at a fixed concentration of the other component. This leads to an enhancement on the ability of the dispersions to reduce the interfacial tension. Furthermore, the results show a pronounced synergistic impact of the interaction between chitosan and silica nanoparticles on the reduction of the interfacial tension. This means that the adsorption of the mixed dispersions results in a more pronounced in the interfacial tension of the liquid/air interface than that observed for the adsorption of the individual components. This synergistic adsorption is analogous to that observed by Maestro et al. [53] and Arriaga et al. [54] for the adsorption at the dispersion/air interface of silica nanoparticles decorated with an alkyltrimethylammonium bromide surfactant and silica nanoparticles decorated with n-amylamine, respectively. However, this synergistic adsorption contrasts with the findings by Eftekhari et al. [55] for silica nanoparticles decorated with an alkyltrimethylammonium bromide surfactant. They observed that the addition of particles increases the interfacial tension in relation to the values corresponding for the surfactant.

At low chitosan concentration and fixed nanoparticle concentration, chitosan-capped silica nanoparticles shows a very reduced surface activity, and therefore a reduced interfacial coverage can be expected. This results in an almost negligible reduction of the interfacial tension in comparison to that of the pristine water/air interface. However, an increase in the chitosan concentration in the dispersion, with a fixed silica concentration, results in a significant enhancement of the surface activity of the capped-silica nanoparticles. This can be explained by the fact that as the chitosan concentration increases, the hydrophobization of the nanoparticles is enough to increase their surface activity and promote their adsorption to the aqueous dispersion/air interface.[27]

3.3. Surface dilational response of chitosan-capped silica nanoparticle layers at the dispersion/air interface

The study of the damping of electrically excited capillary waves the dispersion/air interface, caused by the presence of chitosan-capped nanoparticle layers, offers valuable insights into the dilational interfacial rheological behavior at frequencies exceeding 50 Hz. These measurements provide critical information on the kinetic processes occurring within the adsorbed layer, such as the redistribution of chitosan molecules between the nanoparticles and the fluid/fluid

interface, or the structural reorganization within the adsorbed layer.[45] To investigate these phenomena, electrocapillary wave experiments were performed across a frequency range of 60-450 Hz. Frequencies beyond 450 Hz could not be explored due to a significant decrease in signal intensity, which substantially impacted the sensitivity of the measurements.

The spatial profile of a capillary wave excited at an arbitrary point on a fluid/fluid interface (xy plane), which is defined as coordinate x = 0, can be described in terms of a damped cosine wave, given by the following expression,

$$u_z = u_z^0 e^{-\beta x} cos\left(\frac{2\pi}{\lambda} + \phi\right), \quad (1)$$

where u_z^0 is the wave amplitude, and β and λ are the damping coefficient and the characteristic wavelength of the capillary wave, respectively. ϕ accounts for the phase lag. **Figure 4** shows the frequency (v) dependence of the damping coefficients and the characteristic wavelengths corresponding to layers of chitosan-capped silica nanoparticles adsorbed at the dispersion/air interface.

The results suggest that at a constant frequency, the capillary wavelength λ, exhibits minimal variation with increasing particle concentration, regardless of the chitosan concentration. However, this variation becomes more pronounced as the chitosan concentration increases (see inserted panels in **Figures 4a and 4b**). These observations can be interpreted using Kelvin's law ($\lambda^3 = 2\pi\gamma/v^2\rho$, where ρ represents the bulk density). Kelvin's law is a first-order approximation valid strictly for low-viscosity simple liquid surfaces [56]. Indeed, the higher the particle concentration, the lower the interfacial tension, which in turn results in a lower value of the capillary wavelength. Conversely, the layers obtained from dispersion with lower values of c_{CHI}=5 mM yield higher λ values than when the chitosan concentration is higher (c_{CHI}=10 mM). This phenomenon can also be explained by considering that for fixed nanoparticle concentration, the interfacial tension assumes higher values as the polymer concentration decreases (see **Figure 3**).

The interpretation of the frequency dependencies of the damping coefficient is less straightforward (see **Figures 4c and 4d**). For the damping coefficient at the highest chitosan concentration studied (c_{CHI}=10 mM), there are no effect of the particle concentration. In contrast, for dispersions with a chitosan concentration of 5 mM, the damping coefficient values remain relatively constant at low frequencies, showing no significant variation (i.e., they overlap within the combined error bars) as the particle concentration changes. However, at higher frequencies, the damping coefficient decreases as the particle concentration increases. Furthermore, an increase in polymer concentration results in an increase in the value of the damping coefficient for a fixed silica nanoparticle concentration. This can be understood by considering a derivation

of Stokes's law ($\beta = 4\eta\omega/3\gamma$, where η represents the solution viscosity). This predicts, for the surface of low viscosity pure liquids, an increase in the damping coefficient with the increase in the viscosity (viscosity data for chitosan solutions and chitosan-capped silica nanoparticle dispersions are reported in Table 1). In addition, the reduction in the interfacial tension resulting from the increase in the polymer concentration should consequently result in an increase in the damping coefficient. Additionally, it must be expected that the increase in the surface concentration will also contribute to the enhanced damping coefficient due to the viscoelastic character of the monolayer.

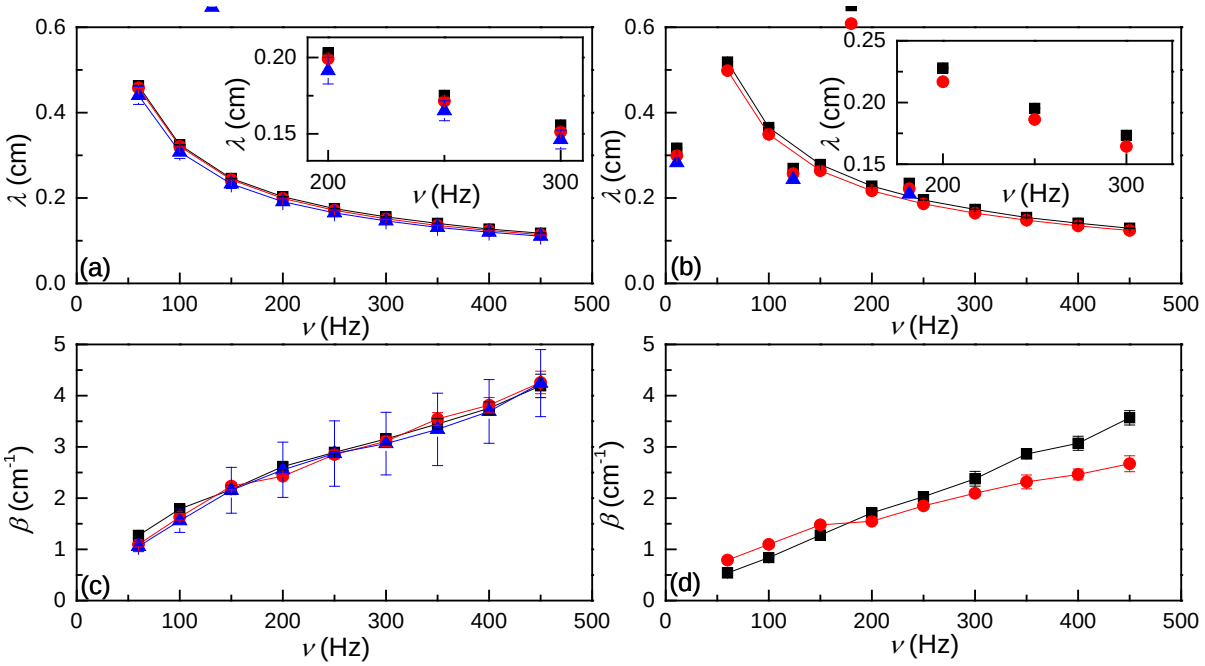

Figure 4. Frequency dependences of the wavelength (λ) and damping (β) for layers obtained from the adsorption of dispersions of chitosan-capped silica nanoparticles, with different chitosan and silica nanoparticles concentrations, at the dispersion/air interface (pH=4.5). (a, b) λ values for layers obtained from the adsorption of dispersions with chitosan concentrations 10 mM and 5 mM, respectively, and (c,d) β values for layers obtained from the adsorption of dispersions with chitosan concentrations 10 mM and 5 mM, respectively. The figures inserted in panels a and b represent a zoom of the frequency dependences of the wavelength (λ) in the frequency range 200-300 Hz. In the different panels, the lines are guides for the eyes, and the different symbols refer to different nanoparticle concentrations: (■) c_{NPs}=0 %w/w, (●) c_{NPs}=0.5 %w/w and (▲) c_{NPs}=1 %w/w. The data reported correspond to the average of three independent measurements.

Table 1. Viscosity data for chitosan solutions and chitosan-capped particle dispersions at pH=4.5 as were obtained by using a Ubbelohde viscometer. Notice that only stable chitosan-capped particle dispersions were measured. The data reported correspond to the average of three independent measurements.

c_{CHI} (mM)	η (mPa.s) c_{NPs}=0%w/w	η (mPa.s) c_{NPs}=0.4%w/w	η (mPa.s) c_{NPs}=0.5%w/w	η (mPa.s) c_{NPs}=1.0%w/w
2	1.5±0.1	-	-	-
4	3.04±0.2	2.01±0.1	-	-
5	3.5±0.3	-	2.4±0.2	-
10	5.1±0.5	-	4.5±0.5	4.1±0.5

The modification of the damping coefficient with the particle concentration reveals the existence of two different regimes, as evidenced by the results. At a high chitosan concentration (c_{CHI}=10 mM), the damping coefficient remains almost constant regardless of the silica nanoparticles concentration. This can be understood by considering that at such high chitosan concentration, the variation of the solution viscosity is minimal with the increase in the particle concentration. Conversely, when the concentration of chitosan is reduced to 5 mM, the viscosity exhibits a more pronounced decrease with the increase in the particle concentration, resulting in a corresponding decrease in the damping coefficient with the particle concentration.

A more detailed examination of the frequency dependence of the capillary wavelength and the damping coefficient (see **Figure 5**) reveals that the experimental data are consistent with the predictions of simple scaling laws: $q \sim \omega^a$ and $\beta \sim \omega^b$, where $\omega=2\pi\nu$ represents the angular frequency and $q=2\pi/\lambda$ is the wavevector. In this analysis, the exponent a was found to be in the range 0.67-0.69 under all conditions studied, which is in close agreement with the prediction of Kelvin's law: $q \sim \omega^{2/3}$. In contrast, the exponent for the scaling law describing the frequency dependence of β differs from the predicted value derived from the Stoke's law (b~1).[56] This is undoubtedly related to viscoelastic character of the interfacial layer.

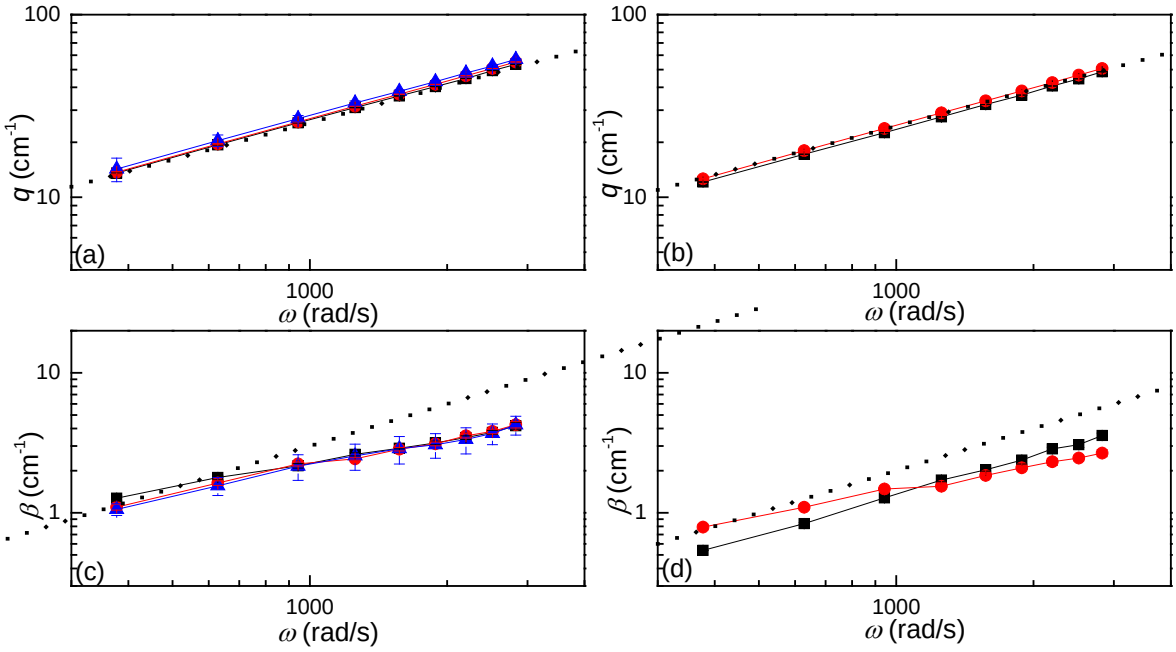

Figure 5. Representation of the dependences of q and β on the angular wavelength for layers obtained from the adsorption of dispersions of chitosan-capped silica nanoparticles, with different chitosan and silica nanoparticles concentrations, at the dispersion/air interface (pH=4.5). (a, b) q values for layers obtained from the adsorption of dispersions with chitosan concentrations 10 mM and 5 mM, respectively, and (c,d) β values for layers obtained from the adsorption of dispersions with chitosan concentrations 10 mM and 5 mM, respectively. In the different panels, the solid lines are guides for the eyes, and the different symbols refer to different nanoparticle concentrations: (■) c_{NPs}=0 %w/w, (●) c_{NPs}=0.5 %w/w and (▲) c_{NPs}=1 %w/w. On the other hand, the dotted black line represents the ideal scaling behavior described by Kelvin ($q \sim \omega^a$ with a~2/3) and Stokes laws ($\beta \sim \omega^b$ with b~1) for q and β, respectively. The data reported correspond to the average of three independent measurements.

To determine the dilational response of a monolayer from electrocapillary wave experiments, it is essential to numerically solve the dispersion equation, $D(q, \omega) = 0$. This equation connects the characteristics of transverse wave propagation —angular frequency ω, wavelength λ, and damping coefficient β— with the monolayer's constitutive parameters, including interfacial tension (γ), dilational storage modulus (ε_r), and dilational viscosity (κ) [57,58,59].

$$D(q,\omega) = T(q,\omega,\gamma)L(q,\omega,\varepsilon) + C(q,\omega). \quad (2)$$

The underlying premise is that the dilational rheological behavior of layers at the water/air interface can be characterized in terms of the interaction between the transverse or capillary component, $T(q,\omega,\gamma)$, and the longitudinal or dilational component $L(q,\omega,\varepsilon)$. In this context,

$C(q,\omega)$ accounts for the coupling between transverse (capillary) and longitudinal (dilational) waves.[59] By solving the dispersion equation, it becomes possible to compute the dilational viscoelastic modulus as

$$\varepsilon(\omega) = \varepsilon_r(\omega) + i\varepsilon_i(\omega) = \varepsilon(\omega) = \left. \frac{-(\eta\omega(q-m))^2}{\gamma q^2 + i\eta\omega(q+m) - \frac{\rho}{q}\omega^2} - i\eta\omega(q+m) \right/ q^2, \quad (3)$$

with $q = \frac{2\pi}{\lambda} - i\beta$ being the complex wavevector and $m = \sqrt{q^2 + i\omega\frac{\rho}{\eta}}$ the capillary penetration depth (Re(m) > 0). Accurately extracting the constitutive parameters of monolayers from electrocapillary wave measurements presents significant challenges. These challenges primarily arises from the varying sensitivity of capillary waves to the dilational properties of the interface. The resonance condition suggests that when the frequency of dilational modes is close to that of the capillary modes, the sensitivity of capillary waves in determining the interfacial dilational elastic modulus (ε_r) and the interfacial dilational viscous modulus (ε_i) is maximized. In first approximation, the resonance occurs under the following condition,

$$\left(\frac{\varepsilon_r}{\gamma}\right)_R = 0.10 - 0.15. \quad (4)$$

The subscript *R* denotes the resonance condition, which is crucial for the accurate determination of dilational parameters from electrocapillary wave experiments. When the ε_r/γ ratio deviates from the resonance condition, the uncertainty in the dilational parameters obtained from the experimental data analysis increases significantly. In the case of the experiments performed in this work, $\varepsilon_r/\gamma > (\varepsilon_r/\gamma)_R$, which introduces a large uncertainty in the determination on the determination of the viscoelastic parameters of the interface. This uncertainty increases as the ε_r/γ increases. Therefore, assuming that the interfacial tension is a constant for a specific dispersion of capped particles, the uncertainty in the determination is expected to increase as the in the interfacial dilational elastic modulus increases. This can be understood by considering that, far from the resonance, a small variation in the input values of γ and η introduces a large uncertainty in the determination of the interfacial dilational viscoelastic moduli.

Figure 6 shows the frequency dependence of the interfacial dilational elastic (ε_r) and viscous (ε_i) moduli corresponding to layers of chitosan-capped silica nanoparticles at the dispersion/air interface. These were obtained for the adsorption of dispersions with increasing concentrations of silica nanoparticles and a fixed concentration of chitosan (10 mM).

The experimental data indicates that, except for chitosan solutions (c_{NPs}=0%w/w), the storage component of the dilational viscoelastic response, i.e., the elastic modulus, of the nanocomposite layer is higher than the viscous modulus within the entire frequency range. In

the particular case of chitosan layers, $\varepsilon_r > \varepsilon_i$ at the lowest frequencies, where ε_r becomes comparable to ε_i at the highest frequencies probed. Therefore, it can be assumed that chitosan layers pass from a mainly elastic behavior to a gel-like one with the increase of the frequency. On the other hand, the storage contribution for nanocomposite layers is higher than that observed for chitosan (see **Figure 6a**), whereas the opposite is true for the viscous modulus. This can be assumed to be the result of the different structure of the layers. Pure chitosan layers at the solution/air dispersion present the capacity to reorganize at the interface and dissipate the energy associated with the interfacial deformation through the reorganization of the polymer chains. This phenomenon is less pronounced when the nanocomposite layers are considered, as most of the chitosan is expected to be attached to the particles, and therefore its reorganization within the interface is very limited. Additionally, the dilational deformation of the interface is expected to contribute to the packing of the particles at the interface, which presents a more limited capacity to reorganize. This, in turn, contributes to the increase of the importance of the elastic component of the dilational response.

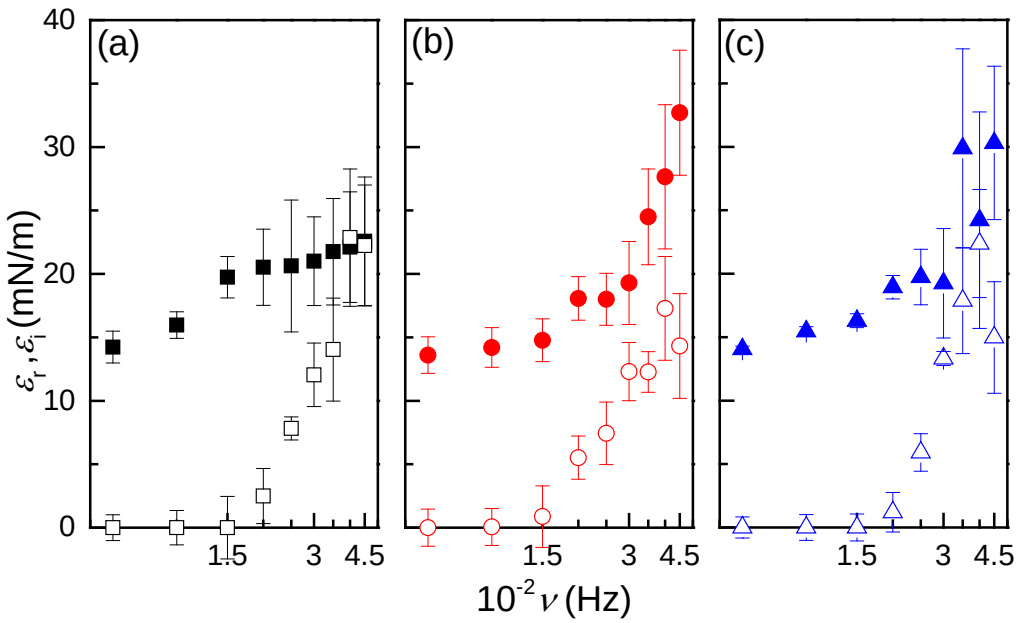

Figure 6. Frequency dependences of the interfacial elastic (ε_r) and viscous (ε_i) moduli obtained from electrocapillary wave experiments for layers obtained from the adsorption of dispersions of chitosan-capped silica nanoparticles, with different silica nanoparticles concentrations and a fixed chitosan concentration (10 mM), at the dispersion/air interface (pH=4.5). (a) c_{NPs}=0%w/w. (b) c_{NPs}=0.5%w/w. (c) c_{NPs}=1.0%w/w. In all the panels solid symbols represent ε_r values and open symbols represent ε_i.The data reported correspond to the average of three independent measurements.

The aforementioned scenario differs when the chitosan concentration is reduced to 5 mM, as shown in **Figure 7**. Indeed, under these conditions, the chitosan layer displays predominantly elastic behavior ($\varepsilon_i \sim 0$, irrespectively of the probed frequency), whereas in the case of the chitosan-silica nanoparticle composite layer, the elastic and viscous moduli differ significantly at low frequencies. However, they assume very similar values at the highest probed frequencies. This can be understood by considering that in the case of chitosan layer, the low chitosan concentration allows the chitosan to attach at the interface in an extended conformation. Consequently, the viscous dissipation resulting from the presence of segments protruding into the air phase is strongly hindered. On the other hand, the different behavior on the viscoelastic response of the composite layer in relation to layers with higher chitosan concentration can be ascribed to the fact that the higher the concentration of chitosan in the mixed dispersion, the more pronounced the interparticle packing at the interface, which is a consequence of the cross-linking between the chitosan-capping layers. This results in an increase in the values of the elastic modulus as the chitosan concentration increases in the mixed dispersion. On the other hand, the viscous modulus increases with the chitosan concentration for chitosan layers, whereas it appears relatively independent on the chitosan concentration with the nanocomposite layers are considered. It is important to note that the values of the dilational elastic modulus, which exceeds the viscous modulus across the studied frequency range, suggest that these layers can resist deformation and maintain structural integrity under dynamic conditions. Such properties play a very important role for stabilizing foams, where the elastic nature of the interfacial film is critical for preventing bubble coalescence and collapse.

A more detailed analysis of the dilational viscoelastic moduli reveals the existence of a relaxation process with a characteristic frequency in the range of 10^2 Hz for particle-laden films. Given the frequency range in which this relaxation occurs, it cannot be ascribed to a diffusion-controlled adsorption of the particles at the interface, which should appear in the frequency region below 1 Hz.[45] Consequently, the relaxation observed in the dilational response is likely associated with a kinetic process occurring within the interface. This may be attributed to the reorganization of the chitosan chains attached to the particles, or even to free chitosan molecules co-adsorbed at the interface together with the chitosan-capped particles. It is unlikely that this kinetic process at the interface can be associated with a time-dependent reorganization of the particles at the interface, which may appear at frequencies closer to that corresponding to the diffusion from the bulk to the interface.[45] Unfortunately, the limited accessible experimental window provided by the electrocapillary measurements performed in this work does not allow for a more detailed analysis of the relaxation process occurring within the

interfacial films. To overcome the limitations imposed by the experimental window of ECW measurements, future studies could integrate complementary techniques in the low frequency range (oscillatory interfacial rheology or capillary pressure tensiometry) and high frequency ranges (surface quasi-elastic ligth scattering) to capture a broader range of relaxation processes [60]. Additionally, advancements in instrumental sensitivity and theoretical modeling would enhance the precision and applicability of ECW data for analyzing complex interfacial systems, allowing the extension of the experimental window.

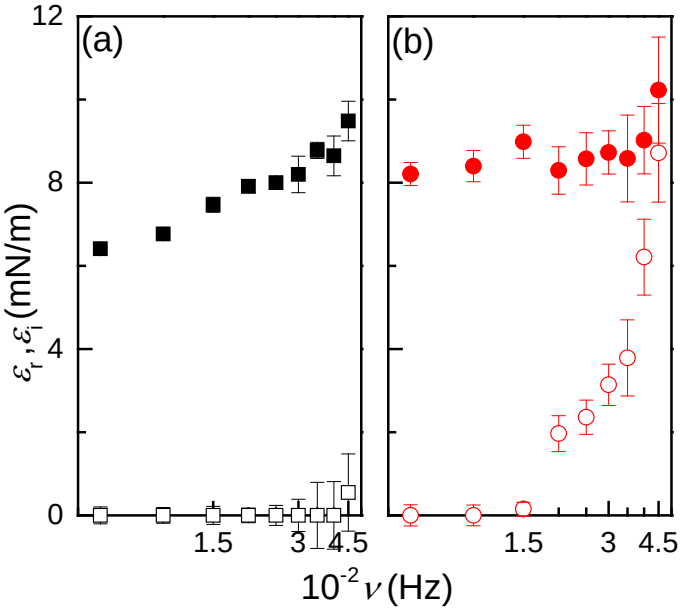

Figure 7. Frequency dependences of the interfacial elastic (ε_r) and viscous (ε_i) moduli obtained from electrocapillary wave experiments for layers obtained from the adsorption of dispersions of chitosan-capped silica nanoparticles, with different silica nanoparticles concentrations and a fixed chitosan concentration (5 mM), at the dispersion/air interface (pH=4.5). (a) c_{NPs}=0%w/w. (b) c_{NPs}=0.5%w/w. In all the panels solid symbols represent ε_r values and open symbols represent ε_i.The data reported correspond to the average of three independent measurements.

4. Conclusions

The adsorption of chitosan on silica nanoparticles has a significant impact on the hydrophobicity and charge properties of the nanoparticles. At pH 4.5, optimal adsorption occurs due to the strong positive charge of chitosan and the negative charge of silica nanoparticles, which facilitate electrostatic interactions. This optimal pH was selected for the evaluation of the stability of chitosan-silica nanoparticle dispersions and their capacity to adsorb at the water/air interface. The compositional map at pH 4.5 indicated the presence of two distinct stability regions for these dispersions, separated by an instability region prone to rapid phase

separation. This instability is attributed to the neutralization of the silica nanoparticle surface charge by adsorbed chitosan, which reaches an isoelectric point where colloidal stability is lost, resulting in sedimentation of the particles. Furthermore, an increase in chitosan concentration beyond this point results in charge inversion and the formation of positively charged chitosan-capped nanoparticles, as evidenced by electrophoretic mobility measurements. Pristine silica nanoparticles exhibited a negative ζ potential, whereas those capped with chitosan displayed positive values, confirming the chitosan adsorption and resulting charge alterations.

The adsorption studies conducted at the aqueous dispersion/air interface showed that chitosan has a significant impact on reducing interfacial tension, which contrasts with the negligible surface activity observed for bare silica nanoparticles. The interfacial tension was observed to decrease with increasing chitosan concentration, which serves to illustrate chitosan's amphiphilic nature and its role in enhancing the surface activity of the nanoparticles. This synergistic effect results in a more pronounced reduction in interfacial tension than would be expected from the individual components.

The damping of electrocapillary waves experiments provided insights into the interfacial rheology of chitosan-capped nanoparticle layers. The presence of these nanoparticles resulted in alterations to both the capillary wavelength and the damping coefficient. At higher concentrations of particles, a reduction in interfacial tension and capillary wavelength was observed. The damping coefficient exhibited a dependence on both particle and chitosan concentrations. At elevated chitosan concentrations, the viscosity of the dispersions increased, resulting in an enhanced damping. Additionally, the surface excess of the layer formed was expected to be higher, contributing to the observed increase in damping. The frequency dependence of the interfacial dilatational elastic and viscous moduli revealed that nanocomposite layers exhibited a higher elastic modulus in comparison to pure chitosan layers. This can be attributed to the restricted capacity of composite layers at the interface for reorganization, which consequently increases the importance of the elastic response. Overall, the study highlights the critical role of pH in modulating chitosan adsorption on silica nanoparticles, the resulting phase behavior, surface charge modifications, and enhanced interfacial properties of the composites. In addition, the mainly elastic character of the formed layers and the enhanced adsorption capabilities observed suggest that these nanocomposite layers are well-suited for stabilizing foams and emulsions, where interfacial viscoelasticity and tension reduction are critical factors. Potential applications include food-grade foams, pharmaceutical emulsions, and cosmetic formulations, where stability and biocompatibility are paramount.

Acknowledgements

This work was performed in the framework of the European Innovative Training Network-Marie Sklodowska-Curie Action NanoPaInt (grant agreement 955612) funded by the E.U. The work by the group in Madrid was also supported under grants PID2023-147156NB-I00, funded by MCIN/AEI/10.13039/501100011033 (Spain), and PR12/24-31566 (Ayudas para la financiación de proyectos de investigación UCM 2023). We thank the Unidad de Espectroscopía y Correlación (CAI de Técnicas Químicas of the UCM) for the use of their facilities.

References

[1] B.P. Binks, Colloidal Particles at a Range of Fluid–Fluid Interfaces, Langmuir 33 (2017) 6947–6963. https://doi.org/10.1021/acs.langmuir.7b00860.

[2] E. Guzmán, F. Martínez-Pedrero, C. Calero, A. Maestro, F. Ortega, R.G. Rubio, A broad perspective to particle-laden fluid interfaces systems: from chemically homogeneous particles to active colloids, Adv. Colloid Interface Sci. 302 (2022) 102620. https://doi.org/10.1016/j.cis.2022.102620.

[3] A. Maestro, E. Santini, E. Guzmán, Physico-chemical foundations of particle-laden fluid interfaces, The European Physical Journal E 41 (2018) 97. https://doi.org/10.1140/epje/i2018-11708-6.

[4] E. Guzmán, I. Abelenda-Núñez, A. Maestro, F. Ortega, A. Santamaria, R.G. Rubio, Particle-laden fluid/fluid interfaces: physico-chemical foundations, J. Phys.: Cond. Matter 33 (2021) 333001. https://doi.org/10.1088/1361-648X/ac0938.

[5] M. Zanini, L. Isa, Particle contact angles at fluid interfaces: pushing the boundary beyond hard uniform spherical colloids, Journal of Physics: Condensed Matter 28 (2016) 313002. https://doi.org/10.1088/0953-8984/28/31/313002.

[6] A. V Bayles, J. Vermant, Divide, Conquer, and Stabilize: Engineering Strong Fluid–Fluid Interfaces, Langmuir 38 (2022) 6499–6505. https://doi.org/10.1021/acs.langmuir.2c00948.

[7] J. Vialetto, M. Anyfantakis, Exploiting Additives for Directing the Adsorption and Organization of Colloid Particles at Fluid Interfaces, Langmuir 37 (2021) 9302–9335. https://doi.org/10.1021/acs.langmuir.1c01029.

[8] N. Ballard, A.D. Law, S.A.F. Bon, Colloidal particles at fluid interfaces: behaviour of isolated particles, Soft Matter 15 (2019) 1186–1199. https://doi.org/10.1039/C8SM02048E.

[9] A. Maestro, Tailoring the interfacial assembly of colloidal particles by engineering the mechanical properties of the interface, Curr. Opin. Colloid Interface Sci. 39 (2019) 232–250. https://doi.org/10.1016/j.cocis.2019.02.013.

[10] A. Maestro, E. Guzmán, F. Ortega, R.G. Rubio, Contact angle of micro- and nanoparticles at fluid interfaces, Curr Opin Colloid Interface Sci 19 (2014) 355–367. https://doi.org/10.1016/j.cocis.2014.04.008.

[11] Y. Lin, H. Skaff, T. Emrick, A.D. Dinsmore, T.P. Russell, Nanoparticle Assembly and Transport at Liquid-Liquid Interfaces, Science (1979) 299 (2003) 226–229. https://doi.org/10.1126/science.1078616.
[12] J. Forth, P.Y. Kim, G. Xie, X. Liu, B.A. Helms, T.P. Russell, Building Reconfigurable Devices Using Complex Liquid–Fluid Interfaces, Advanced Materials 31 (2019) 1806370. https://doi.org/10.1002/adma.201806370.
[13] V. Garbin, Colloidal particles: Surfactants with a difference, Phys. Today 66 (2013) 68–69. https://doi.org/10.1063/PT.3.2158.
[14] V. Garbin, J.C. Crocker, K.J. Stebe, Nanoparticles at fluid interfaces: Exploiting capping ligands to control adsorption, stability and dynamics, J Colloid Interface Sci 387 (2012) 1–11. https://doi.org/https://doi.org/10.1016/j.jcis.2012.07.047.
[15] Y. Yan, Y. Cai, X. Liu, G. Ma, W. Lv, M. Wang, Hydrophobic Modification on the Surface of SiO_2 Nanoparticle: Wettability Control, Langmuir 36 (2020) 14924–14932. https://doi.org/10.1021/acs.langmuir.0c02118.
[16] N.C. Starvaggi, B.J. Bradford, C.D.L. Taylor, E.B. Pentzer, Wettability-tuned silica particles for emulsion-templated microcapsules, Soft Matter 19 (2023) 7635–7643. https://doi.org/10.1039/D3SM00860F.
[17] H.-T. Rong, S. Frey, Y.-J. Yang, M. Zharnikov, M. Buck, M. Wühn, C. Wöll, G. Helmchen, On the Importance of the Headgroup Substrate Bond in Thiol Monolayers: A Study of Biphenyl-Based Thiols on Gold and Silver, Langmuir 17 (2001) 1582–1593. https://doi.org/10.1021/la0014050.
[18] R. Songolzadeh, J. Moghadasi, Stabilizing silica nanoparticles in high saline water by using ionic surfactants for wettability alteration application, Colloid Polym. Sci. 295 (2017) 145–155. https://doi.org/10.1007/s00396-016-3987-3.
[19] E. Santini, E. Guzmán, M. Ferrari, L. Liggieri, Emulsions stabilized by the interaction of silica nanoparticles and palmitic acid at the water-hexane interface, Colloids Surf. A 460 (2014) 333–341. https://doi.org/10.1016/j.colsurfa.2014.02.054.
[20] A. González-González, N. Sánchez-Arribas, E. Santini, J.L. Rodríguez-Villafuerte, C. Carbone, F. Ravera, F. Ortega, L. Liggieri, R.G. Rubio, E. Guzmán, Effects of Oil Phase on the Inversion of Pickering Emulsions Stabilized by Palmitic Acid Decorated Silica Nanoparticles, Colloids and Interfaces 6 (2022) 27. https://doi.org/10.3390/colloids6020027.
[21] G. Sun, T. Guo, J. Luo, R. Liu, T. Ngai, B.P. Binks, Phase Inversion of Pickering Emulsions Induced by Interfacial Electrostatic Attraction, Langmuir 39 (2023) 1386–1393. https://doi.org/10.1021/acs.langmuir.2c02048.
[22] M. Anyfantakis, J. Vialetto, A. Best, G.K. Auernhammer, H.-J. Butt, B.P. Binks, D. Baigl, Adsorption and Crystallization of Particles at the Air–Water Interface Induced by Minute Amounts of Surfactant, Langmuir 34 (2018) 15526–15536. https://doi.org/10.1021/acs.langmuir.8b03233.
[23] J. Jiang, Y. Zhu, Z. Cui, B.P. Binks, Switchable Pickering Emulsions Stabilized by Silica Nanoparticles Hydrophobized In Situ with a Switchable Surfactant, Angew. Chem. Int. Ed. 52 (2013) 12373–12376. https://doi.org/10.1002/anie.201305947.
[24] B.P. Binks, L. Isa, A.T. Tyowua, Direct Measurement of Contact Angles of Silica Particles in Relation to Double Inversion of Pickering Emulsions, Langmuir 29 (2013) 4923–4927. https://doi.org/10.1021/la4006899.
[25] A. Maestro, E. Guzmán, E. Santini, F. Ravera, L. Liggieri, F. Ortega, R.G. Rubio, Wettability of silica nanoparticle-surfactant nanocomposite interfacial layers, Soft Matter 8 (2012). https://doi.org/10.1039/c1sm06421e.

[26] L. Alison, A.F. Demirörs, E. Tervoort, A. Teleki, J. Vermant, A.R. Studart, Emulsions Stabilized by Chitosan-Modified Silica Nanoparticles: pH Control of Structure–Property Relations, Langmuir 34 (2018) 6147–6160. https://doi.org/10.1021/acs.langmuir.8b00622.
[27] L. Alison, P.A. Rühs, E. Tervoort, A. Teleki, M. Zanini, L. Isa, A.R. Studart, Pickering and Network Stabilization of Biocompatible Emulsions Using Chitosan-Modified Silica Nanoparticles, Langmuir 32 (2016) 13446–13457. https://doi.org/10.1021/acs.langmuir.6b03439.
[28] G.S. Luengo, A.-L. Fameau, F. Léonforte, A.J. Greaves, Surface science of cosmetic substrates, cleansing actives and formulations, Adv. Colloid Interface Sci. 290 (2021) 102383. https://doi.org/10.1016/j.cis.2021.102383.
[29] G.S. Luengo, F. Leonforte, A. Greaves, R.G. Rubio, E. Guzman, Physico-chemical challenges on the self-assembly of natural and bio-based ingredients on hair surfaces: towards sustainable haircare formulations, Green Chem. 25 (2023) 7863–7882. https://doi.org/10.1039/D3GC02763E.
[30] L. Fernández-Peña, E. Guzmán, F. Leonforte, A. Serrano-Pueyo, K. Regulski, L. Tournier-Couturier, F. Ortega, R.G. Rubio, G.S. Luengo, Effect of molecular structure of eco-friendly glycolipid biosurfactants on the adsorption of hair-care conditioning polymers, Colloids Surf B Biointerfaces 185 (2020). https://doi.org/10.1016/j.colsurfb.2019.110578.
[31] I. Aranaz, A.R. Alcántara, M.C. Civera, C. Arias, B. Elorza, A. Heras Caballero, N. Acosta, Chitosan: An Overview of Its Properties and Applications, Polymers (Basel) 13 (2021) 3256. https://doi.org/10.3390/polym13193256.
[32] C.P. Jiménez-Gómez, J.A. Cecilia, Chitosan: A Natural Biopolymer with a Wide and Varied Range of Applications, Molecules 25 (2020) 3981. https://doi.org/10.3390/molecules25173981.
[33] J. Wang, S. Zhuang, Chitosan-based materials: Preparation, modification and application, J. Clean. Product. 355 (2022) 131825. https://doi.org/10.1016/j.jclepro.2022.131825.
[34] M. Azmana, S. Mahmood, A.R. Hilles, A. Rahman, M.A. Bin Arifin, S. Ahmed, A review on chitosan and chitosan-based bionanocomposites: Promising material for combatting global issues and its applications, Int. J. Biological Mol. 185 (2021) 832–848. https://doi.org/10.1016/j.ijbiomac.2021.07.023.
[35] F. Heidari, S.M. Jafari, A.M. Ziaiifar, N. Anton, Surface modification of silica nanoparticles by chitosan for stabilization of water-in-oil Pickering emulsions, Carbohydr. Polym. Technol. Appl. 6 (2023) 100381. https://doi.org/10.1016/j.carpta.2023.100381.
[36] F. Nan, J. Wu, F. Qi, Y. Liu, T. Ngai, G. Ma, Uniform chitosan-coated alginate particles as emulsifiers for preparation of stable Pickering emulsions with stimulus dependence, Colloids Surf. A 456 (2014) 246–252. https://doi.org/10.1016/j.colsurfa.2014.05.017.
[37] P. Wongkongkatep, K. Manopwisedjaroen, P. Tiposoth, S. Archakunakorn, T. Pongtharangkul, M. Suphantharika, K. Honda, I. Hamachi, J. Wongkongkatep, Bacteria Interface Pickering Emulsions Stabilized by Self-assembled Bacteria–Chitosan Network, Langmuir 28 (2012) 5729–5736. https://doi.org/10.1021/la300660x.
[38] S. Zhang, Y. Zhou, C. Yang, Pickering emulsions stabilized by the complex of polystyrene particles and chitosan, Colloids Surf. A 482 (2015) 338–344. https://doi.org/10.1016/j.colsurfa.2015.06.029.

[39] X. Hu, Y. Wang, B. Peng, Chitosan-Capped Mesoporous Silica Nanoparticles as pH-Responsive Nanocarriers for Controlled Drug Release, Chem. Asian J. 9 (2014) 319–327. https://doi.org/10.1002/asia.201301105.
[40] I.A. Sogias, V. V. Khutoryanskiy, A.C. Williams, Exploring the Factors Affecting the Solubility of Chitosan in Water, Macromol. Chem. Phys. 211 (2010) 426–433. https://doi.org/10.1002/macp.200900385.
[41] F. Ravera, E. Santini, G. Loglio, M. Ferrari, L. Liggieri, Effect of Nanoparticles on the Interfacial Properties of Liquid/Liquid and Liquid/Air Surface Layers, J. Phys. Chem. B 110 (2006) 19543–19551. https://doi.org/10.1021/jp0636468.
[42] I. Varga, R.A. Campbell, General Physical Description of the Behavior of Oppositely Charged Polyelectrolyte/Surfactant Mixtures at the Air/Water Interface, Langmuir 33 (2017) 5915–5924. https://doi.org/10.1021/acs.langmuir.7b01288.
[43] A. Puente-Santamaría, F. Ortega, A. Maestro, R.G. Rubio, E. Guzmán, Non-equilibrium states in polyelectrolyte-surfactant systems at fluid interfaces: A critical review, Curr. Opin. Colloid Interface Sci. 71 (2024) 101804. https://doi.org/10.1016/j.cocis.2024.101804.
[44] M. Smoluchowski, Handbuch der Elektrizität und des Magnetismus, Barth-Verlag, Leipzig, Germany, 1921.
[45] L. Liggieri, E. Santini, E. Guzmán, A. Maestro, F. Ravera, Wide-frequency dilational rheology investigation of mixed silica nanoparticle-CTAB interfacial layers, Soft Matter 7 (2011) 7699–7709. https://doi.org/10.1039/c1sm05257h.
[46] A. Maestro, F. Ortega, R.G. Rubio, M.A. Rubio, J. Krägel, R. Miller, Rheology of poly(methyl methacrylate) Langmuir monolayers: Percolation transition to a soft glasslike system, J. Chem. Phys. 134 (2011) 104704. https://doi.org/10.1063/1.3560612.
[47] A. Maestro, Dymanics of interfacial systems, PhD Thesis, Universidad Complutense de Madrid, 2009.
[48] P.R. Van Tassel, Polyelectrolyte adsorption and layer-by-layer assembly: Electrochemical control, Curr. Opin. Colloid Interface Sci. 17 (2012) 106–113. https://doi.org/10.1016/j.cocis.2011.08.008.
[49] H.M. Fares, J.B. Schlenoff, Equilibrium Overcompensation in Polyelectrolyte Complexes, Macromolecules 50 (2017) 3968–3978. https://doi.org/10.1021/acs.macromol.7b00665.
[50] R. He, J. Chen, C. Zhang, D. Lu, L. Zhang, T. He, Quantification of overcompensated cations in layer-by-layer membrane by Orange yellow II, Sep. Purif. Technol. 331 (2024) 125637. https://doi.org/10.1016/j.seppur.2023.125637.
[51] J. Nilsen-Nygaard, S. Strand, K. Vårum, K. Draget, C. Nordgård, Chitosan: Gels and Interfacial Properties, Polymers (Basel) 7 (2015) 552–579. https://doi.org/10.3390/polym7030552.
[52] V. Babak, I. Lukina, G. Vikhoreva, J. Desbrières, M. Rinaudo, Interfacial properties of dynamic association between chitin derivatives and surfactants, Colloids Surf. A 147 (1999) 139–148. https://doi.org/10.1016/S0927-7757(98)00752-3.
[53] A. Maestro, E. Rio, W. Drenckhan, D. Langevin, A. Salonen, Foams stabilised by mixtures of nanoparticles and oppositely charged surfactants: relationship between bubble shrinkage and foam coarsening, Soft Matter 10 (2014) 6975–6983. https://doi.org/10.1039/C4SM00047A.
[54] L.R. Arriaga, W. Drenckhan, A. Salonen, J.A. Rodrigues, R. Íñiguez-Palomares, E. Rio, D. Langevin, On the long-term stability of foams stabilised by mixtures

of nano-particles and oppositely charged short chain surfactants, Soft Matter 8 (2012) 11085. https://doi.org/10.1039/c2sm26461g.
[55] M. Eftekhari, K. Schwarzenberger, S.I. Karakashev, N.A. Grozev, K. Eckert, Oppositely charged surfactants and nanoparticles at the air-water interface: Influence of surfactant to nanoparticle ratio, J. Colloid Interface Sci. 653 (2024) 1388–1401. https://doi.org/10.1016/j.jcis.2023.09.038.
[56] D. Langevin, Light Scattering by Liquid Surfaces and Complementary Techniques, Marcel Dekker, New York, NY, USA, 1992. https://api.semanticscholar.org/CorpusID:135599440.
[57] V.G. Levich, Physicochemical Hydrodynamics, Prentice-Hall, Englewood Cliffs, NJ, USA, 1962.
[58] E.H. Lucassen-Reynders, J. Lucassen, Properties of capillary waves, Adv Colloid Interface Sci 2 (1970) 347–395. https://doi.org/10.1016/0001-8686(70)80001-X.
[59] F. Ravera, M. Ferrari, E. Santini, L. Liggieri, Influence of surface processes on the dilational visco-elasticity of surfactant solutions, Adv. Colloid Interface Sci. 117 (2005) 75–100. https://doi.org/10.1016/j.cis.2005.06.002.
[60] A.J. Mendoza, E. Guzmán, F. Martínez-Pedrero, H. Ritacco, R. G. Rubio, F. Ortega, V.M. Starov, R. Miller, Particle laden fluid interfaces: Dynamics and interfacial rheology, Adv. Colloid Interface Sci. 206 (2014) 303-319. https://doi.org/10.1016/j.cis.2013.10.010.